Atmospheric Environment 361 (2025) 121482

Contents lists available at ScienceDirect

Atmospheric Environment

journal homepage: www.elsevier.com/locate/atmosenv

Revealing severely underestimated hydrolysis in liquid-phase degradation of alkyl nitrates

Weina Zhang [a,b,*], Yao Zhou [a,b], Ruijing Li [a,b], Dayuan Zheng [a,b], Yuemeng Ji [a,b], Guiying Li [a,b], Taicheng An [a,b]

[a] Guangdong Key Laboratory of Environmental Catalysis and Health Risk Control, Guangdong-Hong Kong-Macao Joint Laboratory for Contaminants Exposure and Health, Institute of Environmental Health and Pollution Control, Guangdong University of Technology, Guangzhou, 510006, China
[b] Guangdong Basic Research Center of Excellence for Ecological Security and Green Development, School of Environmental Science and Engineering, Guangdong University of Technology, Guangzhou, 510006, China

HIGHLIGHTS

- Hydrolysis in previous experiments was underestimated by 80 % in the pH 4–8.
- IPN and NPN lifetimes were underestimated by five orders of magnitude at pH 8.
- Light absorption by aerosols in oceanic and desert regions should be considered.

GRAPHICAL ABSTRACT

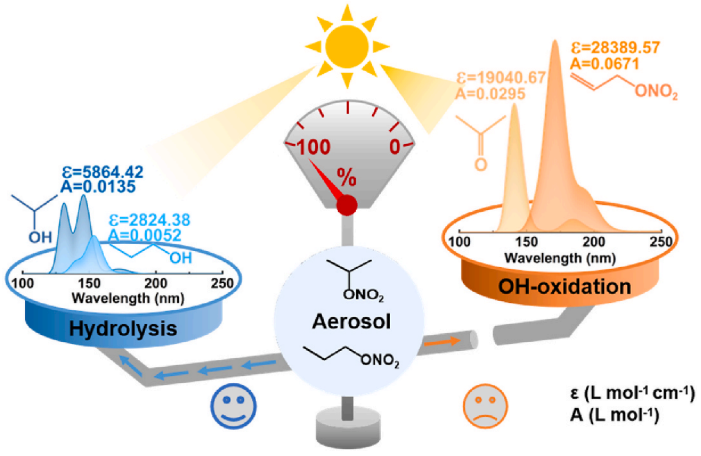

ARTICLE INFO

Keywords:
Particulate alkyl nitrate
Hydrolysis
Oxidation
Competition mechanism
Aerosol optical property

ABSTRACT

Organic nitrates (ONs) are crucial constituents of secondary organic aerosols (SOAs). The liquid-phase degradation of ONs alters the light-absorbing properties of aerosols, thereby influencing the direct radiative effect (DRE) and climate dynamics. Alkyl nitrates (ANs) contribute most of ONs. Previous studies have shown that hydrolysis and •OH-initiated oxidation are two competing degradation pathways for ANs, with oxidation being the dominant mechanism under weakly acidic or weakly alkaline conditions. However, experimental •OH concentrations (ppm) are ten orders of magnitude higher than actual, likely underestimating hydrolysis's contribution. Using propyl nitrate isomers as proxies, we combined liquid chromatography-mass spectrometry and quantum calculations to re-explore AN's degradation at pH 1–8. Our results show that hydrolysis dominates at realistic •OH levels. Specifically, compared to previous experimental results, hydrolysis is underestimated by

* Corresponding author. Guangdong Key Laboratory of Environmental Catalysis and Health Risk Control, Guangdong-Hong Kong-Macao Joint Laboratory for Contaminants Exposure and Health, Institute of Environmental Health and Pollution Control, Guangdong University of Technology, Guangzhou, 510006, China.
E-mail address: zhangwn@gdut.edu.cn (W. Zhang).

https://doi.org/10.1016/j.atmosenv.2025.121482
Received 19 March 2025; Received in revised form 29 July 2025; Accepted 5 August 2025
Available online 6 August 2025

80 % under pH 4–8, resulting in underrating AN's lifetime by 5 orders. Consequently, the resulting light-absorbing attenuation of aerosol will be disregarded, possibly leading to inaccurate DRE and climate effect assessments in oceanic/desert regions where aerosols at pH 4–8 predominates. Our research emphasizes the need to re-evaluate the role of hydrolysis in predicting the fate of ANs and the light-absorbing properties of aerosols.

1. Introduction

Particulate organic nitrates (ONs) constitute 5–44 % of the mass of secondary organic aerosols (SOA) (Fisher et al., 2016; Li et al., 2022; Yang et al., 2024). Previous studies have shown that alkyl nitrates (ANs) play a crucial role in the composition of particulate ONs (Aruffo et al., 2022; Lee et al., 2015; Perring et al., 2013; Song et al., 2018; Zhang et al., 2019). Hydrolysis reactions and liquid-phase oxidation reactions are the primary degradation pathways for particulate ANs (Takeuchi and Ng, 2019; Hansen et al., 2023; Zare et al., 2019). The relevant degradation products will change the light-absorbing property of aerosols (Li et al., 2021; Zhang et al., 2024), which furthermore causes direct radiative effect (DRE) of aerosols. Therefore, investigating the degradation mechanisms of particulate ANs is essential for accurately assessing their climatic impacts.

However, the liquid-phase degradation mechanism of ANs remains poorly understood. In the aerosol liquid phase, the hydrolysis reaction is one of the degradation pathways of ANs, and the degradation products are alcohol and nitric acid (Baker and Easty, 1952; Liu et al., 2012; Wang et al., 2021). Prior studies have confirmed that ANs can undergo hydrolysis reactions with H_2O, H_3O^+, and OH^- in aerosols (Keshavarz et al., 2021; Xi et al., 2023; Zhao et al., 2023). For different molecular structures of ANs, the rate constants of hydrolysis reactions with H_3O^+ are higher than those of hydrolysis reactions initiated by H_2O and OH^- by 4–13 and 8–15 orders of magnitude, respectively (Zhao et al., 2023). The main hydrolysis reaction is determined by aerosol pH (Rindelaub et al., 2015). Generally, the aerosol pH fluctuates within the range of 4–6, showing weak acidity (Karydis et al., 2021). However, in some special environments, the aerosol pH may decrease or increase, thus showing strong acidity or weak alkalinity. For example, during the deliquescence of aerosols containing sulfates and nitrates, the pH range is 1–3, and the aerosol is strongly acidic (Morales et al., 2021). In addition, the concentration of alkaline ions in aerosols in desert and ocean regions is relatively high, making the aerosols weakly alkaline with a pH = 7–8 (Karydis et al., 2021). These observational data indicate that the aerosol pH range is within 1–8 (Herrmann et al., 2015; Shi et al., 2017). Theoretical studies have shown that within the realistic aerosol pH range, ANs mainly undergoes hydrolysis reactions with H_3O^+, and the hydrolysis rate of ANs will increase with the enhancement of aerosol acidity (Morales et al., 2021; Rindelaub et al., 2016; Vesto et al., 2022).

In the atmosphere, •OH is prone to undergo oxidation reactions with particulate ANs through interactions with the aerosol surface or diffusion (George and Abbatt, 2010). Under high liquid water content (0.35 g M^{-3}), the •OH-initiated oxidation reaction is the main liquid-phase oxidation pathway of soluble ONs, including ANs, and the degradation products are ketones, aldehydes, secondary organic nitrates, etc (González-Sánchez et al., 2023; Romonosky et al., 2015; Takeuchi and Ng, 2019). Therefore, within the liquid-phase aerosol, the •OH-initiated oxidation reaction may compete with the hydrolysis reaction (Romonosky et al., 2017). Some experiments even have shown that •OH-initiated oxidation is the dominant degradation pathway of ANs (Gonzalez-Sanchez et al., 2021; González-Sánchez et al., 2023). In order to better compare with the bulk solution conditions in our experiment, we used the •OH concentration in cloud droplets to study the competition between the •OH-initiated oxidation and the hydrolysis reaction. However, the concentration of •OH used in these experiments is at ppm level, while the concentration of •OH in the cloud droplets is 1.7×10^{-11} - 1.7×10^{-8} ppm (Ault, 2020; Gonzalez-Sanchez et al., 2021; Li et al., 2023; Tilgner et al., 2013). Consequently, we speculate that this may lead to an overestimation of the •OH-initiated oxidation when competing with hydrolysis reaction of particulate ANs.

To verify this hypothesis, this study systematically investigated the liquid-phase degradation mechanism of two ANs under different pH conditions. Consequently, isopropyl nitrate (IPN) and n-propyl nitrate (NPN) were selected as proxies in this study. Initially, quantum chemical calculations were carried out to elucidate the •OH-initiated oxidation and hydrolysis reactions of ANs, respectively. Simultaneously, the degradation products of ANs are identified using ultra-high-performance liquid chromatography coupled with quadrupole-orbitrap mass spectrometry (UHPLC - Q - Orbitrap - MS), which served to confirm the accuracy of the proposed degradation mechanism. Based on these findings, the competitive relationship between the •OH-initiated oxidation and hydrolysis reactions of ANs under different pH conditions is successfully revealed. Subsequently, the fates of ANs and the impact of their degradation products on the light-absorbing properties of aerosols are thoroughly discussed.

2. Materials and methods

2.1. Quantum chemical calculations

Quantum chemical calculations based on density functional theory (DFT) were used to explore the liquid-phase degradation mechanism of ANs. All DFT calculations were executed using the Gaussian 09 software package (Frisch et al., 2016). The continuum solvation model density (SMD) was used to account for water's solvation effects (Marenich et al., 2009). Geometric optimizations and vibrational frequency calculations of reactants (RCs), transition states (TSs), intermediates (IN), and products (PR) were done at the M06 - 2X/6–311+G(d,p) level (Liu et al., 2023). The chosen functional has been widely and successfully used for estimating potential barriers in gas and condensed phases (Vereecken and Francisco, 2012; Ji et al., 2022). Reactants, intermediates, and products had no imaginary frequencies; TSs had exactly one. Intrinsic Reaction Coordinate (IRC) calculations verified TS - reactant - product connectivity. Single - point energy calculations were performed at the CCSD(T)/aug - cc - pVDZ level. Gibbs free energies (G) at 298.15 K were obtained by combining these with Gibbs correction energies from geometric optimization. Activation energy ($\Delta G^{\neq}$) was defined as G_{TS}-G_{RC}, and reaction heat (ΔG_r) was calculated as $G_{PR/IN}$-G_{RC}.

The traditional transition - state theory (TST) was used to calculate the reaction rate constant (k) for barrier - involved reactions (Galano and Idaboy, 2009). For barrier - less bimolecular reactions, the diffusion - limited rate constant (k_{diff}) was calculated (Shoup et al., 1981).

The light absorption intensity levels were described using the molar absorption coefficient (ε). Upon the reactants and products as previously described, this study combined the time - dependent density functional theory (TD - DFT) (Adamo and Jacquemin, 2013; Zeng et al., 2018) to calculate ε of each substance at the PBE1PBE/6–311+G (nstates = 10) theoretical level. Based on ε values, the light absorption intensity levels are classified as follows: $\varepsilon > 10^4$ represents strong absorption, $10^3 < \varepsilon < 10^4$ indicates relatively strong absorption, $10^2 < \varepsilon < 10^3$ denotes relatively weak absorption, and $\varepsilon < 10^2$ signifies weak absorption (Zhang et al., 2020).

2.2. Experiments

Samples of ANs. IPN (98 %, details in Table S2) and NPN (95 %, details in Table S2) are commercially purchased. The purity of IPN and

NPN was identified by gas chromatography-flame ionization detector (GC - FID) and nuclear magnetic resonance spectroscopy (NMR).

pH effect on degration products of ANs in bulk solution. In polluted or urban cloud droplets, the •OH concentration is typically 1.7 $\times 10^{-10}$ ppm (Ault, 2020; Gonzalez-Sanchez et al., 2021; Li et al., 2023; Tilgner et al., 2013), the water concentration ranges from 1.20 $\times 10^{-6}$ to 8.99 $\times 10^{-5}$ ppm (Jin et al., 2020; Xu et al., 2022), which is 3–5 orders of magnitude higher than the •OH concentration in cloud droplets. To simulate these environmental conditions while accounting for the instrument's detection limit, we used 4.05 ppm of H_2O_2 and 9.00 $\times 10^5$ ppm of water (Table S1). We conducted liquid-phase degradation experiments on IPN and NPN at pH values of 3, 5, 7 and 9. The degradation products and their relative abundances were analyzed using UHPLC - Q - Orbitrap - MS. We analyzed LC - MS data using Xcalibur 4.1.31 software (Thermo Scientific). Chemicals used were 30 % H_2O_2, 36–38 % high-purity hydrochloric acid, 98 % sodium hydroxide, PBS buffer (pH 7.2–7.4), and HPLC - grade methanol. Preparation steps were: (1) Dissolve organic nitrates in methanol to 250 ppm. (2) Adjust PBS buffer pH to 3, 5, 7, 9 using acid and base. (3) Dilute H_2O_2 to 30 ppm. For the reaction, in a 2 mL screw cap vial, add 100 μL of 250 ppm IPN or NPN, 765 μL of pH adjusted buffer, and 135 μL of 30 ppm H_2O_2 to make 1 mL of reaction solution. This configuration ensures the concentrations of various substances in the reaction solution are fully consistent with the concentration requirements for subsequent instrument use.

Analysis by UHPLC - Q - Orbitrap - MS. We used a high - performance LC - MS/MS system (Thermo Scientific Ultimate 3000 LC + Q Exactive Orbitrap MS + ESI source) for qualitative analysis of the prepared reaction solutions, with a pure methanol solution as the blank. Chromatographic separation was performed on a Hypersil Gold C18 column (100 × 2.1 mm, 1.9 μm). The mobile phase (Table S3) was water (eluent A) and methanol (eluent B). The flow rate was 0.25 mL min^{-1}, and the injection volume was 5 μL. The gradient elution program: 0–2 min, eluent B from 5 % to 20 %; 2–8 min, to 95 % and hold for 8 min; 16–20 min, back to 5 %. Mass signals were acquired in both positive and negative ESI modes at +4.0 kV and −3.0 kV (Table S4). The sheath, auxiliary, and sweep gas flow rates were set at 35, 10, and 0 (arbitrary units). The capillary and auxiliary gas heater temperatures were 320 °C and 350 °C. The instrument automatically switched between ion modes, using full MS - dd MS2 scan mode. The first MS was acquired at 70000 FWHM, and the target MS/MS resolution was 175000 FWHM with an

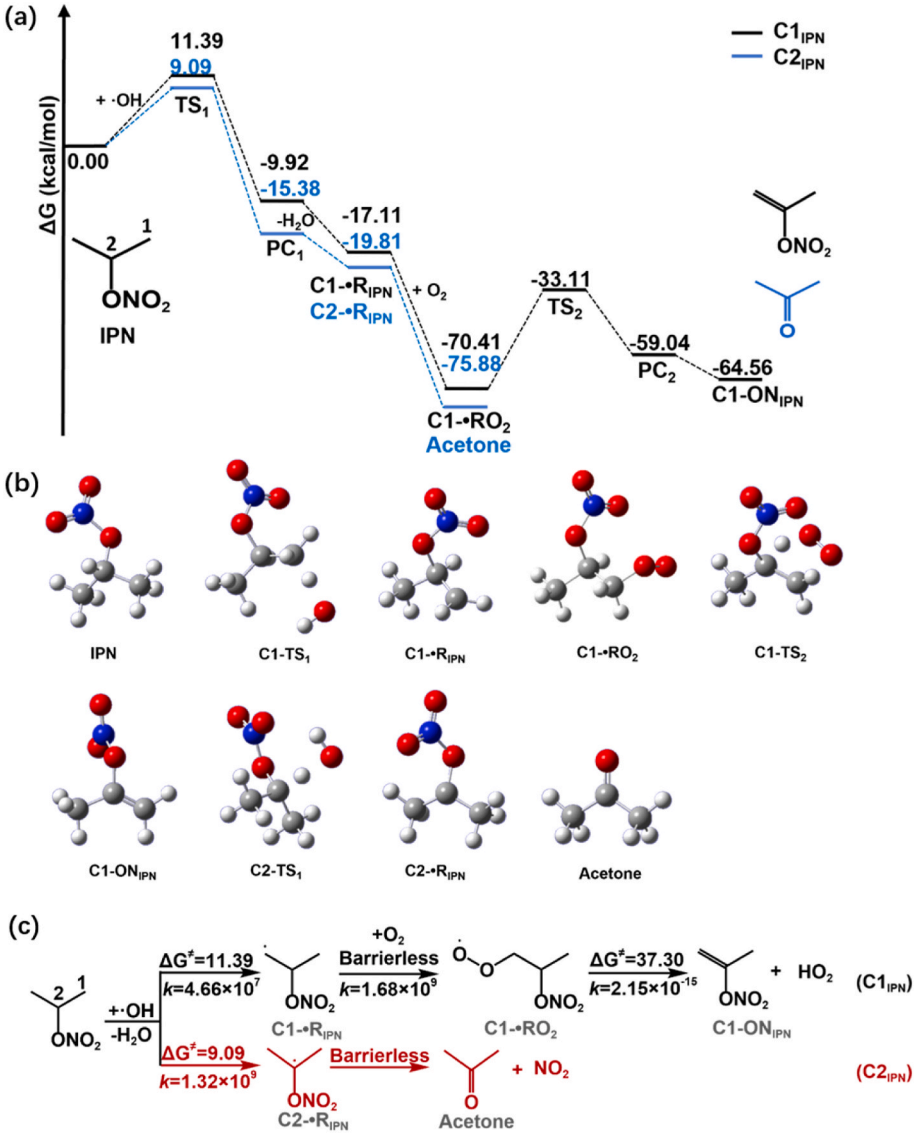

Fig. 1. The •OH-initiated oxidation reaction for isopropyl nitrate (IPN). (a) PES results. (b) Key structures along PES. (c) The •OH-initiated oxidation reaction schematic. The unit of the Gibbs free energy of activation ($\Delta G^{\neq}$) is kcal/mol. For the bimolecular reaction rate constant (k), the unit is M^{-1} s^{-1}, while for the unimolecular reaction k, it is s^{-1}.

isolation width of 0.4 m/z. The m/z scanning range was 50–750.

3. Results and discussion

3.1. •OH-initiated oxidation reaction

First, we compared the •OH-initiated oxidation reaction of these two ANs. For IPN, the corresponding potential energy surface (PES) (Fig. 1a) and key structures (Fig. 1b) are shown in Figures. The hydrogen abstraction occurs at the C1 and C2 positions, leading to two oxidation pathways, namely $C1_{IPN}$ and $C2_{IPN}$ (Fig. 1c). Along the $C1_{IPN}$ pathway, IPN undergoes a series of elementary reactions, including •OH-initiated hydrogen abstraction (Liu et al., 2023; Ng et al., 2017), O_2 addition, and intramolecular hydrogen abstraction (Aschmann et al., 2011, 2012; Deka et al., 2018; Wen et al., 2022), ultimately leading to the formation of the secondary ON (C1-ON_{IPN}, CH_2=C(ONO_2)CH_3). The energy scan results indicate that the O_2 addition step is barrierless (Fig. S1). The $\Delta G^{\neq}$ for the intramolecular hydrogen abstraction step is 37.30 kcal/mol, which is the rate-determining step among the three elementary reactions. This step determines the k of the $C1_{IPN}$ pathway to be 2×10^{-15} s^{-1}, suggesting that the formation of C1-ON_{IPN} is extremely slow.

Conversely, along the $C2_{IPN}$ pathway, IPN first experiences •OH-initiated hydrogen abstraction, followed by a decomposition reaction, finally resulting in the production of acetone. The rate - determining step is the •OH-initiated hydrogen abstraction, with a $\Delta G^{\neq}$ of 9.09 kcal/mol, which determines the k of this pathway to be 1.32×10^{9} M^{-1} s^{-1}. Meanwhile, energy scan results (Fig. S2) show that the decomposition reaction occurs without an energy barrier. During the reaction of IPN, the concentration of [•OH] can be regarded as constant. Given an [•OH] of 1.7×10^{-10} ppm appearing in cloud droplets, the pseudo-first-order rate constant (k_{app}) of the $C2_{IPN}$ pathway is 1.32×10^{-5} s^{-1}, which is 10 orders of magnitude higher than the k of the $C1_{IPN}$ pathway (2×10^{-15} s^{-1}). This clearly demonstrates that acetone is formed far more rapidly than C1-ON_{IPN}.

Moreover, since the rate constants of the first elementary reactions of $C1_{IPN}$ and $C2_{IPN}$ are 4.66×10^{7} and 1.32×10^{9} M^{-1} s^{-1}, respectively, these findings are in good agreement with those reported by González-Sánchez et al. (Gonzalez-Sanchez et al., 2021; González-Sánchez et al., 2023). This determines that the proportions of C1-ON_{IPN} and acetone in the initial oxidation of IPN are 3.41 % and 96.59 %. These results further confirm that the $C2_{IPN}$ pathway is the predominant pathway for the •OH-initiated oxidation of IPN, and acetone is the major oxidation product. Therefore, for IPN, greater attention should be directed towards the environmental impacts caused by acetone.

Unlike IPN, hydrogen abstraction in NPN occurs at the C1, C2, and C3 positions, giving rise to three distinct oxidation pathways: $C1_{NPN}$, $C2_{NPN}$, and $C3_{NPN}$ (Fig. S3). The PES results and key structures are presented in Figs. S4 and S5. In the $C1_{NPN}$ pathway, propanal is produced through a reaction process similar to that of acetone formation from IPN. The $C2_{NPN}$ pathway leads to the generation of the secondary ON (C2-ON_{NPN}, CH_2=$CHCH_2ONO_2$). Similar to the formation of C1-ON_{IPN} from IPN, the O_2 addition step in this pathway is barrierless (Fig. S6). In the $C3_{NPN}$ pathway, C2-ON_{NPN} is also formed, but the O_2 addition step requires overcoming an energy barrier of 23.33 kcal/mol. The remaining reaction steps are identical to those in the formation of C1-ON_{IPN} from IPN. Here, we emphasize the differences between the oxidation reactions of NPN and IPN. Along the $C1_{NPN}$ pathway, the k for the formation of propanal is determined by the initial hydrogen abstraction step, which is 5.23×10^{8} M^{-1} s^{-1}. This implies that propanal can be rapidly formed under actual atmospheric reaction conditions. Regarding C2-ON_{NPN}, which is produced via both the $C2_{NPN}$ and $C3_{NPN}$ pathways, the rate constants of these two pathways are determined by their respective intramolecular hydrogen abstraction steps, with values of 3.11×10^{-11} and 5.09×10^{-11} M^{-1} s^{-1}, respectively. Thus, the overall k for the formation of C2-ON_{NPN} is 8.2×10^{-11} M^{-1} s^{-1}. This indicates that the formation rate of C2-ON_{NPN} is significantly slower than that of propanal under the same conditions. The rate constants of the initial hydrogen abstraction steps in the $C1_{NPN}$, $C2_{NPN}$, and $C3_{NPN}$ pathways are 5.23×10^{8}, 1.21×10^{9}, and 2.78×10^{8} M^{-1} s^{-1}, respectively. These values determine the proportions of the three pathways be 23.78 %, 55.03 %, and 21.19 % in order. Consequently, the proportions of propanal and C2-ON_{NPN} are determined to be 23.78 % and 76.22 %, respectively. Although the formation rate of C2-ON_{NPN} is 19 orders of magnitude slower than that of propanal, the final yield of the former is 3.2 times that of the latter. This suggests that in the NPN degradation reaction dominated by oxidation, the aerosols optical properties caused by propanal should be considered in the initial stage, while the impact of C2-ON_{NPN} should be given more attention in the long - term. In contrast, the oxidation of IPN produces only acetone, so the influence of the IPN oxidation reaction on aerosol properties is solely attributed to acetone.

3.2. Hydrolysis reactions under various pH

ANs may concurrently engage in reactions with H_2O, H_3O^+, and OH^-. Initially, the reaction of IPN with H_2O unfolds through three distinct reaction pathways: unimolecular substitution (S_N1_{IPN}), bimolecular substitution (S_N2_{IPN}), and H_2O addition (H_2O-ad_{IPN}) (Fig. 2a). The PESs corresponding to each pathway are presented in Fig. S7, while the key structures are depicted in Figs. S8–S10. Along the S_N1_{IPN} pathway, a decomposition reaction with a $\Delta G^{\neq}$ of 28.51 kcal/mol is followed by a barrier - less H_2O addition reaction (Fig. S11), ultimately leading to the formation of protonated isopropyl alcohol (IPA). The decomposition reaction serves as the rate-determining step, dictating the k of the S_N1_{IPN} pathway to be 6.37×10^{-9} M^{-1} s^{-1}. Conversely, the S_N2_{IPN} pathway consists of a single elementary reaction. The associated $\Delta G^{\neq}$ is 33.61 kcal/mol, with a k of 2.08×10^{-9} M^{-1} s^{-1}. Distinct from the products of the first two pathways, the H_2O-ad_{IPN} pathway results in the production of isopropyl alcohol. Nevertheless, the $\Delta G^{\neq}$ surges to 57.05 kcal/mol, causing the k to plummet to 1.11×10^{-26} M^{-1} s^{-1}. Under realistic environmental conditions, this pathway can be deemed negligible. Consequently, the principal product of the reaction between IPN and H_2O is protonated isopropyl alcohol, and the corresponding formation k is 8.45×10^{-9} M^{-1} s^{-1}. In the present experiment, the concentration of H_2O, denoted as [H_2O], is 9×10^{5} ppm. As a result, the pseudo - first - order rate constant (k_{app}) of the reaction between IPN and H_2O is 4.23×10^{-7} s^{-1}. This finding suggests that this reaction progresses at a sluggish pace under actual atmospheric conditions.

Secondly, the reaction of IPN with H_3O^+ exclusively proceeds via the S_N1_{IPN} pathway (Fig. 2b). Along this pathway, a sequence of elementary reactions takes place, including protonation, decomposition, and H_2O addition, ultimately culminating in the formation of protonated isopropyl alcohol. Both the protonation reaction and the H_2O addition reaction (Figs. S11–S12) are endothermic processes devoid of an energy barrier, findings that are in accordance with prior reports (Zhao et al., 2023). The decomposition reaction, characterized by $\Delta G^{\neq}$ of 5.97 kcal/mol, acts as the rate - determining step of this pathway. This ascertains that the k for the generation of protonated isopropyl alcohol in this reaction is 2.5×10^{8} s^{-1}, a value 15 orders of magnitude greater than the k_{app} of the reaction between IPN and H_2O. This implies that this reaction pathway can occur within the atmospheric environment.

Finally, the reaction of IPN with OH^- encompasses four distinct pathways: OH^- addition (OH^- - ad_{IPN}), S_N2_{IPN}, hydrogen abstraction at the α - position (H_α-abstraction), and hydrogen abstraction at the β - position (H_β-abstraction) (Fig. 2c). Isopropyl alcohol can be formed through the initial two pathways. Along OH^--ad_{IPN} pathway, the OH^- addition reaction serves as the rate - determining step, with a $\Delta G^{\neq}$ of 24.46 kcal/mol, which dictates the k to be 1.13×10^{-2} M^{-1} s^{-1}. For the S_N2_{IPN} pathway, the $\Delta G^{\neq}$ is 24.61 kcal/mol, resulting in k of 8.76×10^{-3} M^{-1} s^{-1}. Consequently, k for the formation of isopropyl alcohol in the reaction between IPN and OH^- is 2.01×10^{-2} M^{-1} s^{-1}.

Additionally, the H_α-abstraction and H_β-abstraction pathways lead to

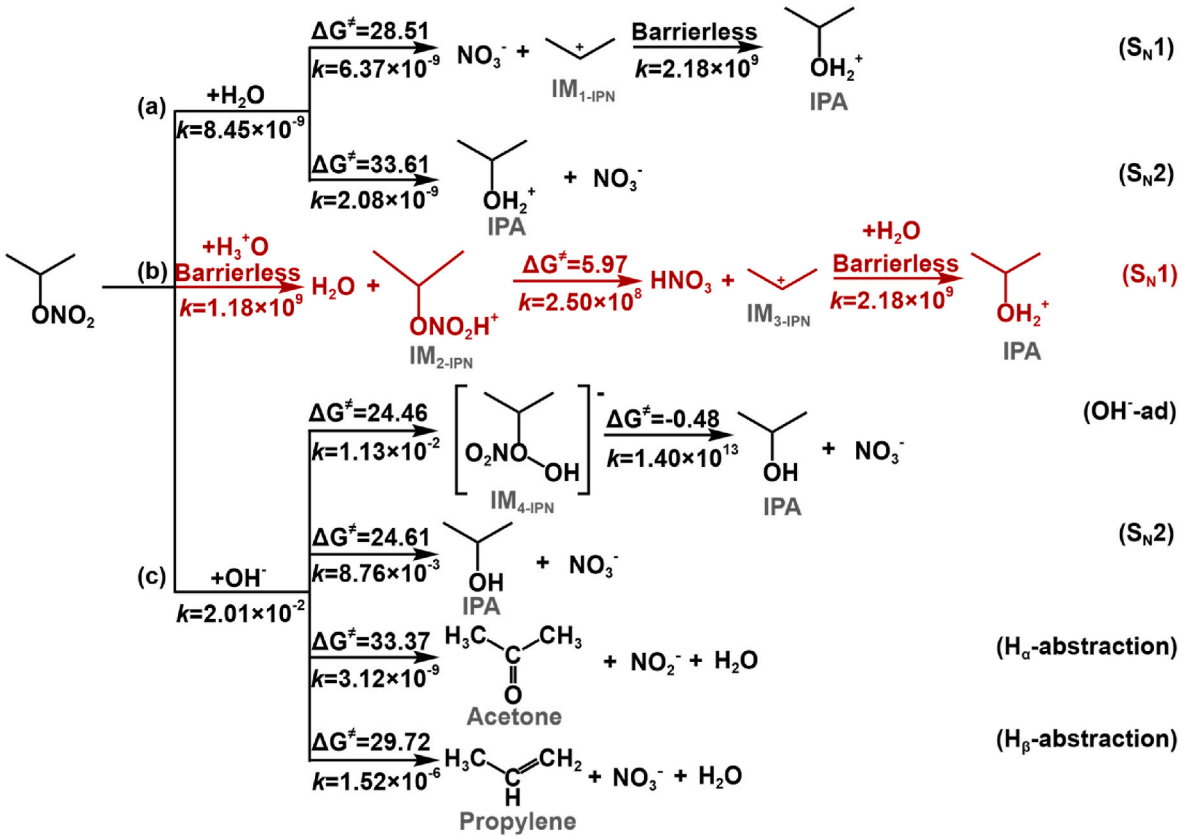

Fig. 2. The hydrolysis reaction pathways between IPN and (a) H_2O, (b) H_3O^+, and (c) OH^-. The unit of the Gibbs free energy of activation ($\Delta G^{\neq}$) is kcal/mol. For the bimolecular reaction rate constant (k), the unit is M^{-1} s^{-1}, while for the unimolecular reaction k, it is s^{-1}.

the production of acetone and propylene, respectively. Nevertheless, the $\Delta G^{\neq}$ values of these two pathways reach as high as 33.37 and 29.72 kcal/mol, respectively, causing k to drop as low as 3.12×10^{-1} and 1.52×10^{-6} M^{-1} s^{-1}. Therefore, the k of the reaction between IPN and OH^- is jointly determined by the OH^--ad_{IPN} and S_N2_{IPN} pathways, amounting to 2.01×10^{-2} M^{-1} s^{-1}. It is further established that the proportion of isopropyl alcohol generated in this reaction is 100 %, whereas the proportions of acetone and propylene are both 0 %.

The findings presented above substantiate that isopropyl alcohol is the principal product when IPN engages in hydrolysis reactions with H_2O, H_3O^+, and OH^-. Subsequently, we computed the variations of the overall hydrolysis rate of IPN and the relative proportions of the three distinct reaction types as a function of pH (Fig. 3a). The results reveal that within the pH range of 1–8, the reaction between IPN and H_3O^+ constitutes 100 % of the hydrolysis processes, thereby acting as the dominant hydrolysis pathway. Significantly, as the solution shifts from a weakly acidic condition (pH > 3) to a strongly acidic regime (pH < 3), the total hydrolysis rate of IPN undergoes a remarkable increase of up to seven orders of magnitude, rising from 2.81×10^{-3} to 2.81×10^{4} M s^{-1}.

The above conclusion is equally valid for the hydrolysis reaction of NPN (Fig. 3b). For a comprehensive and detailed discussion of this topic, please refer to Text S1 (Figs. S13–S17). A notable distinction between the two compounds is that the main hydrolysis product of NPN is propyl alcohol (NPA) rather than isopropyl alcohol. This difference can be attributed to the disparity in the positions of the -ONO_2 groups in IPN and NPN. In summary, the current results indicate that as the acidity of the aerosol intensifies, the hydrolysis reactions of IPN and NPN accelerate significantly. This phenomenon aligns well with the experimental findings reported in the existing literature (Rindelaub et al., 2016; Zhao et al., 2023).

3.3. Contribution of hydrolysis to an degradation

To validate the proposed oxidation and hydrolysis reaction mechanisms, we employed UHPLC - Q - Orbitrap - MS to **precisely characterize** the degradation products of IPN and NPN across a pH range of

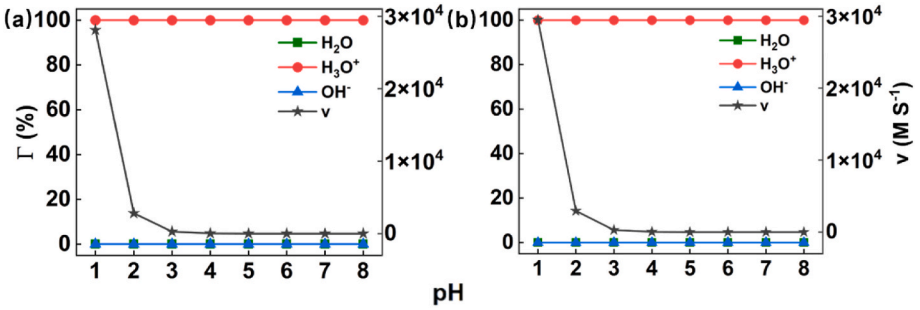

Fig. 3. The proportions (Γ) of the three types of hydrolysis reactions and total hydrolysis reaction rate (v) for (a) IPN and (b) NPN across different pH values.

3–9. In line with the detection constraints of the instrument, and consistent with other experimental studies, we utilized •OH at the ppm level. Under the experimental conditions, **markedly different** degradation products of IPN and NPN were detected at various pH values. For IPN (Fig. 4a), the identified degradation products include isopropyl alcohol (C_3H_8O), hydroxy acetone ($C_3H_6O_2$), and secondary ON ($CH_2{=}C(ONO_2)CH_3$). These products correspond precisely to the hydrolysis and oxidation products of IPN as found in the above quantum chemical calculations, thus confirming the accuracy of the two degradation reaction mechanisms of IPN obtained in this study. Likewise, for the NPN experiment (Fig. 4b), propanal ($C_3H_6O_2$) and secondary ON ($CH_2{=}CHCH_2ONO_2$) are identified, which match the degradation products of NPN predicted by the above theory. This finding attests to the reliability of the current NPN degradation mechanism.

Based on the present degradation mechanism, we furthermore calculate the proportions (Γ) of the hydrolysis reactions of IPN and NPN in their respective total degradation reactions (details in Tables S5–S6):

$$\Gamma = \frac{k_{\text{hydrolysis}}[H_3O^+][AN]}{k_{\text{oxidation}}[\cdot OH][AN] + k_{\text{hydrolysis}}[H_3O^+][AN]} = \frac{k_{\text{hydrolysis}}10^{-pH}}{k_{\text{oxidation}}[\cdot OH] + k_{\text{hydrolysis}}10^{-pH}} \quad (1)$$

where [AN] represents the concentration of either IPN or NPN, [•OH] denotes the concentration dissolved in actual cloud droplets (1.7×10^{-10} ppm) or the concentration used in this experiment (8.1 ppm), and $k_{\text{oxidation}}$ and $k_{\text{hydrolysis}}$ are the overall rate constants of the •OH-initiated oxidation and hydrolysis, respectively. Meanwhile, the pH ranges from 1 to 8, which corresponds to the pH range of atmospheric aerosols (Shi et al., 2017). Consequently, Fig. 5aandb illustrate the changing trends of Γ as the pH increases. The results show that under the experimental conditions with [•OH] = 8.1 ppm, the Γ values of the two ANs exceed 50 % when pH < 3, indicating that the hydrolysis reaction predominates over the oxidation reaction. Conversely, when pH > 4, Γ < 20 %, suggesting a tendency for the oxidation reaction to be the primary degradation pathway. This result is consistent with the findings in the previous studies, which states that the oxidation reaction is the main degradation pathway for ANs (González-Sánchez et al., 2023). However, in the actual cloud droplets environment, the [•OH] is far below the ppm level. According to Equation (1), the •OH-initiated oxidation reactions of IPN and NPN are nearly negligible at real [•OH], while the hydrolysis reaction accounts for 100 %. Evidently, both the current experiment and the previous studies have significantly underestimated the proportion of the hydrolysis reaction in the liquid - phase degradation of ANs. For strongly acidic aerosols (pH < 3), Γ is underestimated by 0–50 %. Particularly for weakly acidic (pH = 4–6) and weakly alkaline (pH = 7–8) aerosols, Γ is underestimated by more than 80 %.

This finding will further result in an underestimation of the lifetimes of IPN and NPN within cloud droplets (Fig. 5c and d). To illustrate, we take IPN as a representative case (Fig. 5c). When the pH is less than 3, the lifetimes of IPN in both the experimental setup and the actual environment fall within the range of 1.17×10^{-8} to 7.57×10^{-7} s. Moreover, at a pH of 4, the actual lifetime of IPN in the cloud droplets should reach 1.17×10^{-5} s, suggesting that the experimentally derived value is underestimated by one order of magnitude. Notably, when the pH further rises to 8, the underestimation of IPN's lifetime becomes more pronounced, reaching up to five orders of magnitude. In summary, as aerosol acidity decreases, the predicted lifetimes of IPN and NPN exhibit greater deviations under the experimentally applied •OH concentration compared to those under cloud droplet conditions.

4. Conclusions and implications

In this study, we selected IPN and NPN as representative alkane - type ONs. By integrating liquid chromatography - mass spectrometry (LC - MS) with theoretical chemical calculations, we conducted a systematic investigation into their liquid - phase degradation mechanisms. Our findings reveal that the •OH-initiated oxidation reaction can only supersede the hydrolysis reaction as the primary sink for ANs when the •OH concentration reaches the ppm level. Nevertheless, in the actual atmospheric environment, the •OH concentration in cloud droplets is 1.7×10^{-11} -1.7×10^{-8} ppm (Ault, 2020; Gonzalez-Sanchez et al., 2021; Tilgner et al., 2013), rendering the contribution of the oxidation

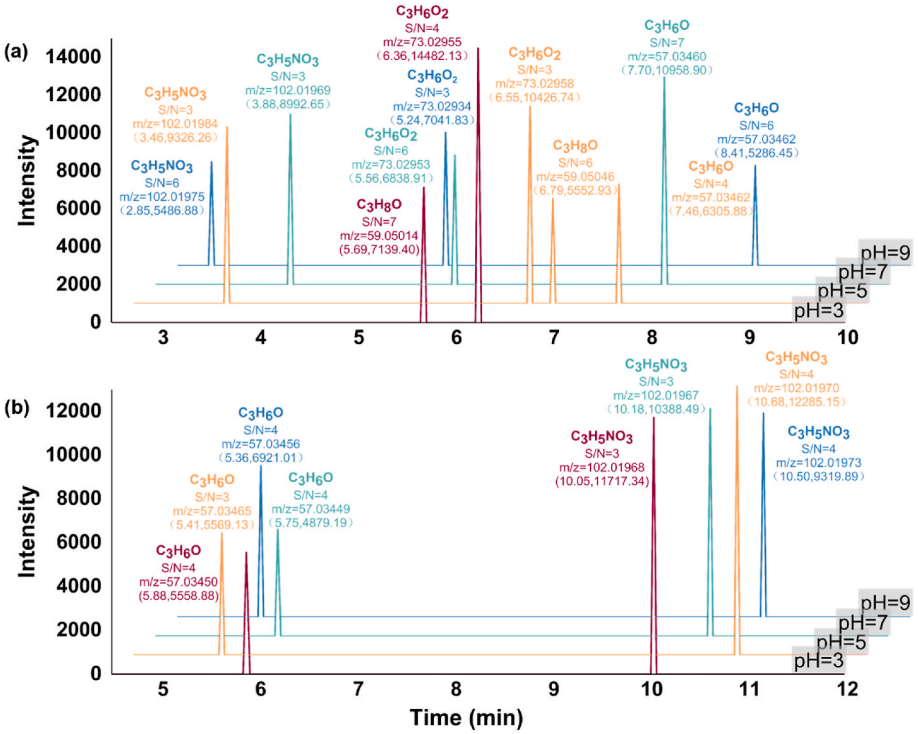

Fig. 4. Extracted ion chromatograms of degradation products of (a) IPN and (b) NPN under different pH conditions.

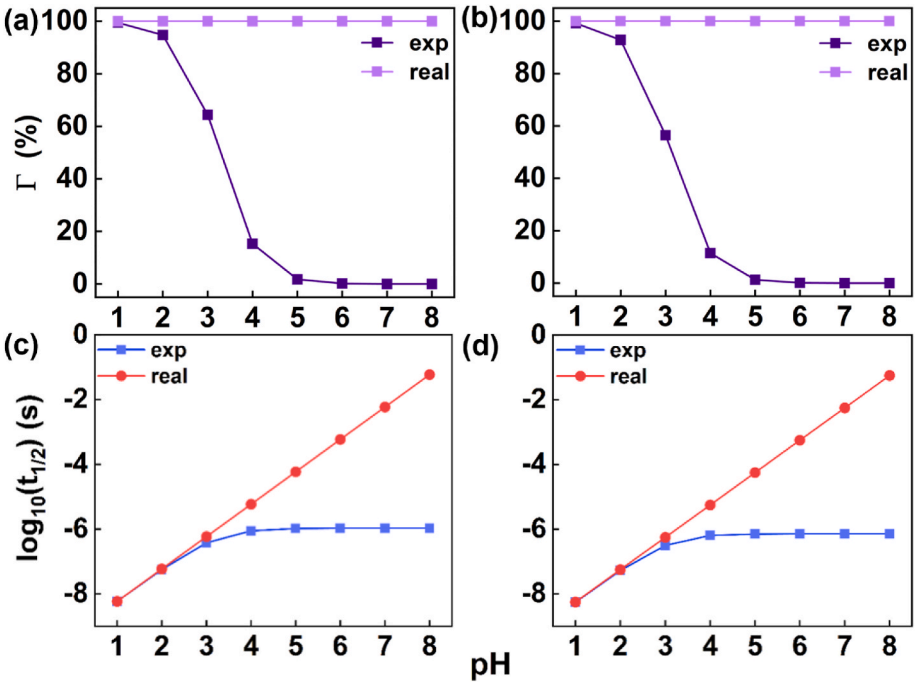

Fig. 5. (a) and (b) the proportion (Γ) of hydrolysis reactions in the total degradation reactions and (c–d) half-lives of IPN (left panel) and NPN (right panel). "exp" means the [·OH] of bulk solution in under experimental conditions, namely 8.1 ppm. "real" means the [·OH] of real cloud droplets, namely 1.7×10^{-10} ppm.

reaction almost negligible. Consequently, we prove that hydrolysis stands as the exclusive degradation pathway for IPN and NPN. Crucially, within the typical pH range of aerosols (pH = 1–8), IPN and NPN predominantly engage in hydrolysis reactions with H_3O^+. The reaction kinetics accelerate as the aerosol acidity intensifies, a phenomenon consistent with previous experimental and theoretical investigations (Keshavarz et al., 2021; Zhao et al., 2023). Our results clearly demonstrate that the significance of hydrolysis reactions in the degradation of particulate ANs has been grossly underestimated. Specifically, for weakly acidic (pH = 4–6) and weakly alkaline (pH = 7–8) aerosols, the contribution of hydrolysis reactions to the degradation of IPN and NPN has been underestimated by at least 80 %, leading to an underestimation of their lifetimes by up to five orders of magnitude. In oceanic/desert regions (Angle et al., 2021; Karydis et al., 2021), the aerosol

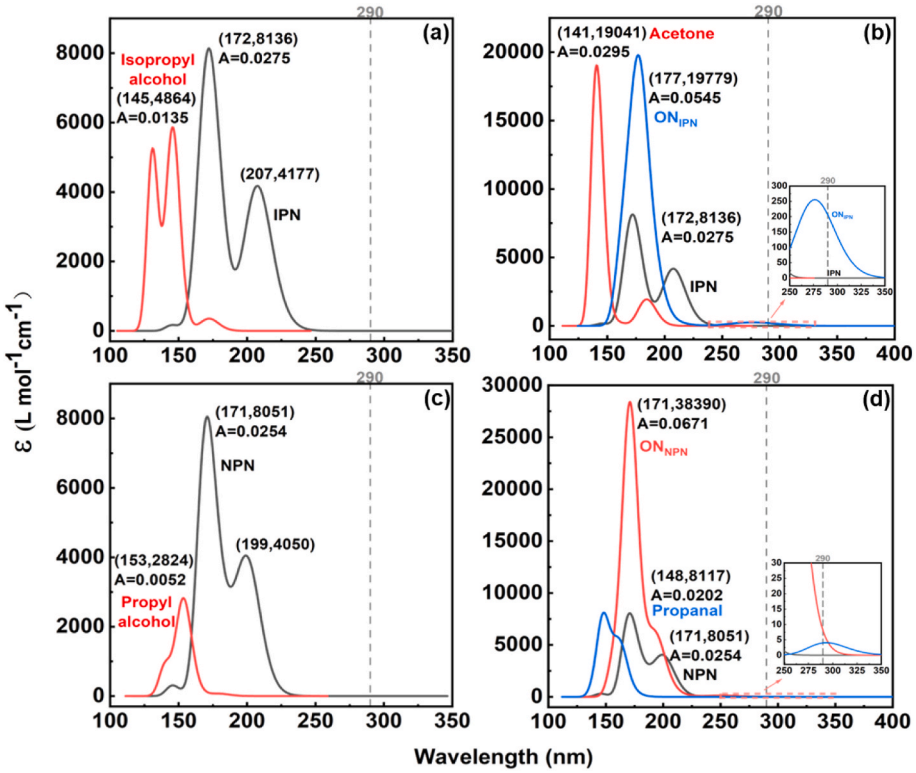

Fig. 6. The absorption spectra changes caused by hydrolysis (left panel) and •OH-initiated oxidation (right panel). The unit of the area A is L mol^{-1}.

pH fluctuates between 4 and 8. Based on our results, hydrolysis emerges as the dominant degradation pathway for IPN and NPN, with isopropyl alcohol and propyl alcohol being the primary degradation products.

Analyses of the molar absorption coefficient (ε) and absorption peak area (A) indicate that hydrolysis reduces the light-absorbing capacity of IPN and NPN aerosols. Taking IPN as an example, the ε_{max} of isopropyl alcohol is 2272 L mol^{-1} cm^{-1} lower than that of IPN, and the A decreases to half of that of IPN (Fig. 6a). In contrast, if the •OH-initiated oxidation were the predominant degradation pathway, as previously hypothesized, an increase in the light - absorbing capacity of IPN and NPN aerosols would be expected. For IPN, its oxidation products, acetone and second - generation organic nitrates, exhibit ε_{max} values 10905 and 11643 L mol^{-1} cm^{-1} higher than that of IPN, respectively, and their combined A is 3.1 times that of IPN (Fig. 6b). Similar trends are observed for NPN (Fig. 6c and d). In addition, the main absorption peaks of the hydrolysis products of IPN and NPN are located in the UVC band ($\leq$290 nm), where solar radiation flux is relatively low. However, the oxidation products of IPN and NPN exhibit notable red-shifted absorption features, with spectral tails extending into the UV–Vis transition range 290–400 nm (UVB - UVA). This means that previous studies which regarded oxidation reactions as the main degradation pathway would overestimate the contribution of ANs to light absorption. This may lead to inaccurate estimation on DRE from ANs (Grace et al., 2020; Heald et al., 2014; Wei et al., 2024). Therefore, under the condition of pH 4–8, the oxidation reaction of ANs is overestimated, which means that the light absorption of aerosols in oceanic and desert environments will be overestimated.

However, present work has some limitations. For instance, other compounds in cloud droplets, such as sulfates, may react with ANs and affect their degradation rate and product distribution (Hu et al., 2011), which is not considered in the present work. In addition to pH factors, the influence of humidity and light intensity over oceans/deserts on the liquid-phase degradation mechanism of ANs should be further investigated. Moreover, quantum chemical calculations are used to reveal liquid-phase degradation mechanism of ANs. However, quantum chemical calculations are limited by scale and cannot fully simulate the environment in real cloud droplets. Therefore, smog chamber experiment and field measurement are necessary to be combined to verify the present work in the future.

CRediT authorship contribution statement

Weina Zhang: Writing – review & editing, Supervision, Project administration, Funding acquisition, Formal analysis. **Yao Zhou:** Writing – original draft, Data curation. **Ruijing Li:** Methodology, Investigation, Formal analysis. **Dayuan Zheng:** Methodology, Formal analysis. **Yuemeng Ji:** Funding acquisition. **Guiying Li:** Methodology, Investigation. **Taicheng An:** Funding acquisition.

Declaration of competing interest

The authors declare that they have no known competing financial interests or personal relationships that could have appeared to influence the work reported in this paper.

Acknowledgements

This work is supported by the NSFC (42020104001, 42277081, and 42077189), the Basic and Applied Basic Research Fund Project of Guangdong Province (2024A1515012691), the National Key Research and Development Program of China (2022YFC3105600), and the Guangzhou Science and Technology Program (2025A04J5188).

Appendix A. Supplementary data

Supplementary data to this article can be found online at https://doi.org/10.1016/j.atmosenv.2025.121482.

Data availability

Data will be made available on request.

References

Adamo, C., Jacquemin, D., 2013. The calculations of excited-state properties with time-dependent density functional theory. Chem. Soc. Rev. 42, 845–856. https://doi.org/10.1039/c2cs35394f.

Angle, K.J., Crocker, D.R., Simpson, R.M.C., Mayer, K.J., Garofalo, L.A., Moore, A.N., Mora Garcia, S.L., Or, V.W., Srinivasan, S., Farhan, M., Sauer, J.S., Lee, C., Pothier, M.A., Farmer, D.K., Martz, T.R., Bertram, T.H., Cappa, C.D., Prather, K.A., Grassian, V.H., 2021. Acidity across the interface from the ocean surface to sea spray aerosol. P. Natl. Acad. Sci. USA. 118. https://doi.org/10.1073/pnas.2018397118.

Aruffo, E., Wang, J., Ye, J., Ohno, P., Qin, Y., Stewart, M., McKinney, K., Di Carlo, P., Martin, S.T., 2022. Partitioning of organonitrates in the production of secondary organic aerosols from alpha-pinene photo-oxidation. Environ. Sci. Technol. 56, 5421–5429. https://doi.org/10.1021/acs.est.1c08380.

Aschmann, S.M., Arey, J., Atkinson, R., 2012. Products of the OH radical-initiated reactions of 2- and 3-hexyl nitrate. Atmos. Environ. 46, 264–270. https://doi.org/10.1016/j.atmosenv.2011.09.073.

Aschmann, S.M., Tuazon, E.C., Arey, J., Atkinson, R., 2011. Products of the OH radical-initiated reactions of 2-propyl nitrate, 3-methyl-2-butyl nitrate and 3-methyl-2-pentyl nitrate. Atmos. Environ. 45, 1695–1701. https://doi.org/10.1016/j.atmosenv.2010.12.061.

Ault, A.P., 2020. Aerosol acidity: novel measurements and implications for atmospheric chemistry. Acc. Chem. Res. 53, 1703–1714. https://doi.org/10.1021/acs.accounts.0c00303.

Baker, J.W., Easty, D.M., 1952. Hydrolytic decomposition of esters of nitric acid. Part I. General experimental techniques.Alkaline hydrolysis and neutral solvolysis of methyl, ethyl, isopropyl, and tert.butyl nitrates in aqueous alcohol. J. Chem. Soc. 217, 1193–1207. https://doi.org/10.1039/jr9520001193.

Deka, R.C., Baruah, S., Deka, A., Gour, N.K., 2018. Theoretical insight of OH-initiated mechanistic pathways and kinetics of n-butyl nitrate ($CH_3CH_2CH_2CH_2ONO_2$) at 298 K and 1 atm. J. Indian Chem. Soc. 95, 9–20.

Fisher, J.A., Jacob, D.J., Travis, K.R., Kim, P.S., Marais, E.A., Miller, C.C., Yu, K., Zhu, L., Yantosca, R.M., Sulprizio, M.P., Mao, J., Wennberg, P.O., Crounse, J.D., Teng, A.P., Nguyen, T.B., St Clair, J.M., Cohen, R.C., Romer, P., Nault, B.A., Wooldridge, P.J., Jimenez, J.L., Campuzano-Jost, P., Day, D.A., Hu, W., Shepson, P.B., Xiong, F., Blake, D.R., Goldstein, A.H., Misztal, P.K., Hanisco, T.F., Wolfe, G.M., Ryerson, T.B., Wisthaler, A., Mikoviny, T., 2016. Organic nitrate chemistry and its implications for nitrogen budgets in an isoprene- and monoterpene-rich atmosphere: constraints from aircraft (SEAC^{4}RS) and ground-based (SOAS) observations in the Southeast US. Atmos. Chem. Phys. 16, 5969–5991. https://doi.org/10.5194/acp-16-5969-2016.

Frisch, M.J., Trucks, G.W., Schlegel, H.B., Scuseria, G.E., Robb, M.A., Cheeseman, J.R., Scalmani, G., Barone, V., Mennucci, B., Petersson, G.A., Nakatsuji, H., Caricato, M., Li, X., Hratchian, H.P., Izmaylov, A.F., J. Bloino, G.Z., Sonnenberg, J.L., Hada, M., Ehara, M., Toyota, K., Fukuda, R., Hasegawa, J., Ishida, M., Nakajima, T., Honda, Y., Kitao, O., Nakai, H., Vreven, T., Montgomery, J.A., Peralta, J.E., Ogliaro, F., Bearpark, M., Heyd, J.J., Brothers, E., Kudin, K.N., Staroverov, V.N., Kobayashi, R., Normand, J., Raghavachari, K., Rendell, A., Burant, J.C., Iyengar, S.S., Tomasi, J., Cossi, M., Rega, N., Millam, J.M., Klene, M., Knox, J.E., Cross, J.B., Bakken, V., Adamo, C., Jaramillo, J., Gomperts, R., Stratmann, R.E., Yazyev, O., Austin, A.J., Cammi, R., Pomelli, C., Ochterski, J.W., Martin, R.L., Morokuma, K., Zakrzewski, V. G., Voth, G.A., Salvador, P., Dannenberg, J.J., Dapprich, S., Daniels, A.D., Farkas, Ö., Foresman, J.B., Ortiz, J.V., Cioslowski, J., Fox, D.J., 2016. Gaussian 09 Wallingford CT.

Galano, A., Idaboy, J.R.A., 2009. Guanosine + OH radical reaction in aqueous solution: a reinterpretation of the UV-vis data based on thermodynamic and kinetic calculations. J. Am. Chem. Soc. 11, 5114–5117. https://doi.org/10.1021/ol901862h.

George, I.J., Abbatt, J.P., 2010. Heterogeneous oxidation of atmospheric aerosol particles by gas-phase radicals. Nat. Chem. 2, 713–722. https://doi.org/10.1038/nchem.806.

González-Sánchez, J.M., Brun, N., Wu, J., Ravier, S., Clément, J.L., Monod, A., 2023. On the importance of multiphase photolysis of organic nitrates on their global atmospheric removal. Atmos. Chem. Phys. 23, 5851–5866. https://doi.org/10.5194/acp-23-5851-2023.

Gonzalez-Sanchez, J.M., Brun, N., Wu, J.T., Morin, J., Temime-Roussel, B., Ravier, S., Mouchel-Vallon, C., Clement, J.L., Monod, A., 2021. On the importance of atmospheric loss of organic nitrates by aqueous-phase center dot OH oxidation. Atmos. Chem. Phys. 21, 4915–4937. https://doi.org/10.5194/acp-21-4915-2021.

Grace, D.N., Lugos, E.N., Ma, S., Griffith, D.R., Hendrickson, H.P., Woo, J.L., Galloway, M.M., 2020. Brown carbon formation potential of the biacetyl–ammonium sulfate reaction system. ACS Earth Space Chem. 4, 1104–1113. https://doi.org/10.1021/acsearthspacechem.0c00096.

Hansen, R.F., Dalton, E.Z., Abney, R.B., Engelhard, M.H., Castillo Valdes, G., Burton, S. D., Chu, R.K., Veghte, D.P., China, S., Losovyj, Y., Cliff, J.B., Raff, J.D., 2023. Reaction of organic matter with nitronium ion as a source of organic nitrate esters in proxies for organic aerosols. ACS Earth Space Chem. 7, 1727–1738. https://doi.org/10.1021/acsearthspacechem.3c00111.

Heald, C.L., Ridley, D.A., Kroll, J.H., Barrett, S.R.H., Cady-Pereira, K.E., Alvarado, M.J., Holmes, C.D., 2014. Contrasting the direct radiative effect and direct radiative forcing of aerosols. Atmos. Chem. Phys. 14, 5513–5527. https://doi.org/10.5194/acp-14-5513-2014.

Herrmann, H., Schaefer, T., Tilgner, A., Styler, S.A., Weller, C., Teich, M., Otto, T., 2015. Tropospheric aqueous-phase chemistry: kinetics, mechanisms, and its coupling to a changing gas phase. Chem. Rev. 115, 4259–4334. https://doi.org/10.1021/cr500447k.

Hu, K.S., Darer, A.I., Elrod, M.J., 2011. Thermodynamics and kinetics of the hydrolysis of atmospherically relevant organonitrates and organosulfates. Atmos. Chem. Phys. 11, 8307–8320. https://doi.org/10.5194/acp-11-8307-2011.

Ji, Y., Shi, Q., Ma, X., Gao, L., Wang, J., Li, Y., Gao, Y., Li, G., Zhang, R., An, T., 2022. Elucidating the critical oligomeric steps in secondary organic aerosol and brown carbon formation. Atmos. Chem. Phys. 22, 7259–7271. https://doi.org/10.5194/acp-22-7259-2022.

Jin, X., Wang, Y., Li, Z., Zhang, F., Xu, W., Sun, Y., Fan, X., Chen, G., Wu, H., Ren, J., Wang, Q., Cribb, M., 2020. Significant contribution of organics to aerosol liquid water content in winter in Beijing, China. Atmos. Chem. Phys. 20, 901–914. https://doi.org/10.5194/acp-20-901-2020.

Karydis, V.A., Tsimpidi, A.P., Pozzer, A., Lelieveld, J., 2021. How alkaline compounds control atmospheric aerosol particle acidity. Atmos. Chem. Phys. 21, 14983–15001. https://doi.org/10.5194/acp-21-14983-2021.

Keshavarz, F., Thornton, J.A., Vehkamäki, H., Kurtén, T., 2021. Reaction mechanisms underlying unfunctionalized alkyl nitrate hydrolysis in aqueous aerosols. ACS Earth Space Chem. 5, 210–225. https://doi.org/10.1021/acsearthspacechem.0c00253.

Lee, L., Wooldridge, P.J., deGouw, J., Brown, S.S., Bates, T.S., Quinn, P.K., Cohen, R.C., 2015. Particulate organic nitrates observed in an oil and natural gas production region during wintertime. Atmos. Chem. Phys. 15, 9313–9325. https://doi.org/10.5194/acp-15-9313-2015.

Li, F., Zhou, S., Du, L., Zhao, J., Hang, J., Wang, X., 2023. Aqueous-phase chemistry of atmospheric phenolic compounds: a critical review of laboratory studies. Sci. Total Environ. 856, 158895. https://doi.org/10.1016/j.scitotenv.2022.158895.

Li, G.B., Cai, S.H., Long, B., 2022. New reactions for the formation of organic nitrate in the atmosphere. ACS Omega 7, 39671–39679. https://doi.org/10.1021/acsomega.2c03321.

Li, J., Han, Z., Sun, Y., Li, J., Liang, L., 2021. Chemical formation pathways of secondary organic aerosols in the Beijing-Tianjin-Hebei region in wintertime. Atmos. Environ. 244. https://doi.org/10.1016/j.atmosenv.2020.117996.

Liu, S., Shilling, J.E., Song, C., Hiranuma, N., Zaveri, R.A., Russell, L.M., 2012. Hydrolysis of organonitrate functional groups in aerosol particles. Aerosol Sci. Technol. 46, 1359–1369. https://doi.org/10.1080/02786826.2012.716175.

Liu, X.H., Meng, T.T., Bai, F.Y., Ni, S., Zhao, Z., 2023. Theoretical investigation on the atmospheric degradation mechanism, kinetics, and fate of hydroxymethyl nitrate initiated by ·OH radicals. New J. Chem. 47, 11414–11424. https://doi.org/10.1039/d3nj01628e.

Marenich, A.V., Cramer, C.J., Truhlar, D.G., 2009. Universal solvation model based on solute electron density and on a continuum model of the solvent defined by the bulk dielectric constant and atomic surface tensions. J. Phys. Chem. 113, 6378–6396. https://doi.org/10.1021/jp810292n.

Morales, A.C., Jayarathne, T., Slade, J.H., Laskin, A., Shepson, P.B., 2021. The production and hydrolysis of organic nitrates from OH radical oxidation of beta-ocimene. Atmos. Chem. Phys. 21, 129–145. https://doi.org/10.5194/acp-21-129-2021.

Ng, M., Mok, D.K.W., Lee, E.P.F., Dyke, J.M., 2017. The atmospherically important reaction of hydroxyl radicals with methyl nitrate: a theoretical study involving the calculation of reaction mechanisms, enthalpies, activation energies, and rate coefficients. J. Phys. Chem. 121, 6554–6567. https://doi.org/10.1021/acs.jpca.7b05035.

Perring, A.E., Pusede, S.E., Cohen, R.C., 2013. An observational perspective on the atmospheric impacts of alkyl and multifunctional nitrates on ozone and secondary organic aerosol. Chem. Rev. 113, 5848–5870. https://doi.org/10.1021/cr300520x.

Rindelaub, J.D., Borca, C.H., Hostetler, M.A., Slade, J.H., Lipton, M.A., Slipchenko, L.V., Shepson, P.B., 2016. The acid-catalyzed hydrolysis of an α-pinene-derived organic nitrate: kinetics, products, reaction mechanisms, and atmospheric impact. Atmos. Chem. Phys. 16, 15425–15432. https://doi.org/10.5194/acp-16-15425-2016.

Rindelaub, J.D., McAvey, K.M., Shepson, P.B., 2015. The photochemical production of organic nitrates from α-pinene and loss via acid-dependent particle phase hydrolysis. Atmos. Environ. 100, 193–201. https://doi.org/10.1016/j.atmosenv.2014.11.010.

Romonosky, D.E., Li, Y., Shiraiwa, M., Laskin, A., Laskin, J., Nizkorodov, S.A., 2017. Aqueous photochemistry of secondary organic aerosol of alpha-pinene and alpha-humulene oxidized with ozone, hydroxyl radical, and nitrate radical. J. Phys. Chem. 121, 1298–1309. https://doi.org/10.1021/acs.jpca.6b10900.

Romonosky, D.E., Nguyen, L.Q., Shemesh, D., Nguyen, T.B., Epstein, S.A., Martin, D.B.C., Vanderwal, C.D., Gerber, R.B., Nizkorodov, S.A., 2015. Absorption spectra and aqueous photochemistry of β-hydroxyalkyl nitrates of atmospheric interest. Mol. Phys. 113, 2179–2190. https://doi.org/10.1080/00268976.2015.1017020.

Shi, G., Xu, J., Peng, X., Xiao, Z., Chen, K., Tian, Y., Guan, X., Feng, Y., Yu, H., Nenes, A., Russell, A.G., 2017. pH of aerosols in a polluted atmosphere: source contributions to highly acidic aerosol. Environ. Sci. Technol. 51, 4289–4296. https://doi.org/10.1021/acs.est.6b05736.

Shoup, D., Lipari, G., Szabo, A., 1981. Diffusion-controlled bimolecular reaction rates. The effect of rotational diffusion and orientation constraints.pdf. Biophys. J. 36, 697–714. https://doi.org/10.1016/s0006-3495(81)84759-5.

Song, J., Zhang, Y., Huang, Y., Ho, K.F., Yuan, Z., Ling, Z., Niu, X., Gao, Y., Cui, L., Louie, P.K.K., Lee, S.C., Lai, S., 2018. Seasonal variations of C_1-C_4 alkyl nitrates at a coastal site in Hong Kong: influence of photochemical formation and oceanic emissions. Chemosphere 194, 275–284. https://doi.org/10.1016/j.chemosphere.2017.11.104.

Takeuchi, M., Ng, N.L., 2019. Chemical composition and hydrolysis of organic nitrate aerosol formed from hydroxyl and nitrate radical oxidation of α-pinene and β-pinene. Atmos. Chem. Phys. 19, 12749–12766. https://doi.org/10.5194/acp-19-12749-2019.

Tilgner, A., Bräuer, P., Wolke, R., Herrmann, H., 2013. Modelling multiphase chemistry in deliquescent aerosols and clouds using CAPRAM3.0i. J. Atmos. Chem. 70, 221–256. https://doi.org/10.1007/s10874-013-9267-4.

Vereecken, L., Francisco, J.S., 2012. Theoretical studies of atmospheric reaction mechanisms in the troposphere. Chem. Soc. Rev. 41, 6259–6293. https://doi.org/10.1039/c2cs35070j.

Vesto, J.I., McAlister, A.B., Wright, K.A., Huang, A., Baldwin, P.R., McLaughlin, Sta, Maria, E.J., LaLonde, R.L., Carrasquillo, A.J., 2022. Condensed phase kinetic studies of hydroxynitrates derived from the photooxidation of carene, limonene, trans-carveol, and perillic alcohol. Atmosphere 13, 592. https://doi.org/10.3390/atmos13040592.

Wang, Y., Piletic, I.R., Takeuchi, M., Xu, T., France, S., Ng, N.L., 2021. Synthesis and hydrolysis of atmospherically relevant monoterpene-derived organic nitrates. Environ. Sci. Technol. 55, 14595–14606. https://doi.org/10.1021/acs.est.1c05310.

Wei, B., Zhang, R., Sit, P.H.L., He, M., Chan, C.K., 2024. Formation and oxidation of imidazole in tropospheric aqueous-phase chemistry: a computational study. ACS. ES&T. Air. 1, 617–627. https://doi.org/10.1021/acsestair.3c00097.

Wen, L., Schaefer, T., Zhang, Y., He, L., Ventura, O.N., Herrmann, H., 2022. T- and pH-dependent OH radical reaction kinetics with glycine, alanine, serine, and threonine in the aqueous phase. Phys. Chem. Chem. Phys. 24, 11054–11065. https://doi.org/10.1039/d1cp05186e.

Xi, X., He, X., Ma, Z.C., Ma, H.Q., Liao, P.C., 2023. Formation processes of nitrogen-containing organic compounds from heterogeneous reactions of $C_3H_6/NO_2/O_3$ with α-Fe_2O_3 particles. Atmos. Environ. 295, 119567. https://doi.org/10.1016/j.atmosenv.2022.119567.

Xu, Y., Dong, X.N., Xiao, H.Y., Zhou, J.X., Wu, D.S., 2022. Proteinaceous matter and liquid water in fine aerosols in Nanchang, Eastern China: seasonal variations, sources, and potential connections. J. Geophys. Res. Atmos. 127. https://doi.org/10.1029/2022jd036589.

Yang, J., Lei, G., Zhu, J., Wu, Y., Liu, C., Hu, K., Bao, J., Zhang, Z., Lin, W., Jin, J., 2024. Particulate-bound alkyl nitrate pollution and formation mechanisms in Beijing, China. Atmos. Chem. Phys. 24, 123–136. https://doi.org/10.5194/acp-24-123-2024.

Zare, A., Fahey, K.M., Sarwar, G., Cohen, R.C., Pye, H.O.T., 2019. Vapor-pressure pathways initiate but hydrolysis products dominate the aerosol estimated from organic nitrates. ACS Earth Space Chem. 3, 1426–1437. https://doi.org/10.1021/acsearthspacechem.9b00067.

Zeng, Y., Shen, Z., Zhang, T., Lu, D., Li, G., Lei, Y., Feng, T., Wang, X., Huang, Y., Zhang, Q., Xu, H., Wang, Q., Cao, J., 2018. Optical property variations from a precursor (isoprene) to its atmospheric oxidation products. Atmos. Environ. 193, 198–204. https://doi.org/10.1016/j.atmosenv.2018.09.017.

Zhang, Q., Shen, Z., Zhang, L., Zeng, Y., Ning, Z., Zhang, T., Lei, Y., Wang, Q., Li, G., Sun, J., Westerdahl, D., Xu, H., Cao, J., 2020. Investigation of primary and secondary particulate Brown carbon in two Chinese cities of Xi'an and Hong Kong in wintertime. Environ. Sci. Technol. 54, 3803–3813. https://doi.org/10.1021/acs.est.9b05332.

Zhang, S., Gao, Y., Xu, X., Chen, L., Wu, C., Li, Z., Li, R., Xiao, B., Liu, X., Li, R., Zhang, F., Wang, G., 2024. Heterogeneous formation and light absorption of secondary organic aerosols from acetone photochemical reactions: remarkably enhancing effects of seeds and ammonia. Atmos. Chem. Phys. 24, 14177–14190. https://doi.org/10.5194/acp-24-14177-2024.

Zhang, Y., Sun, J., Zheng, P., Chen, T., Liu, Y., Han, G., Simpson, I.J., Wang, X., Blake, D. R., Li, Z., Yang, X., Qi, Y., Wang, Q., Wang, W., Xue, L., 2019. Observations of C(1)-C(5) alkyl nitrates in the Yellow River Delta, northern China: effects of biomass burning and oil field emissions. Sci. Total Environ. 656, 129–139. https://doi.org/10.1016/j.scitotenv.2018.11.208.

Zhao, Q., Xie, H.-B., Ma, F., Nie, W., Yan, C., Huang, D., Elm, J., Chen, J., 2023. Mechanism-based structure-activity relationship investigation on hydrolysis kinetics of atmospheric organic nitrates. Npj. Clim. Atmos. Sci. 6, 192. https://doi.org/10.1038/s41612-023-00517-w.